Materials Research Bulletin 95 (2017) 115–122

Contents lists available at ScienceDirect

Materials Research Bulletin

journal homepage: www.elsevier.com/locate/matresbu

Magneto-optical, structural and surface properties of RIB sputtered (Bi, Ga)-substituted DyIG films

A.N. Shaposhnikov[a,*], A.R. Prokopov[a], V.N. Berzhansky[a], A.V. Karavainikov[a], Yu. E. Vysokikh[b], N.N. Gerasimenko[b], D.I. Smirnov[b]

[a] V. I. Vernadsky Crimean Federal University, Simferopol, Russia
[b] National Research University of Electronic Technology, Zelenograd, Moscow, Russia

ARTICLE INFO

Article history:
Received 16 March 2017
Received in revised form 21 June 2017
Accepted 26 June 2017
Available online 13 July 2017

Keywords:
Nanoscale (Bi,Ga)-substituted DyIG films
Reactive ion beam sputtering
Atomic force microscopy

ABSTRACT

The dependences of magneto-optical, structural and morphological properties of reactive ion beam sputtered (RIBS) nanoscale (Bi,Ga)-substituted DyIG [(Bi,Ga:DyIG)] films on (111) GGG and (111) CMZGGG substrates on the time of crystallization annealing were studied using Faraday effect measurements, X-ray diffraction and scanning atomic force microscopy. It was found that the roughness, degree of crystallinity and Faraday rotation angle of the films depend substantially on the substrate type and the time of crystallization annealing. It was determined a minimal time to achieve the optimal ratio between the measured magneto-optical and structural parameters of the film.

1. Introduction

One-dimensional magneto-photonic crystals (1D-MPCs) and the similar multilayer structures have shown many applications in magneto-optical (MO) devices such as magneto-optical modulators [1,2], optical insulators [3,4], magnetic field sensors [5,6] etc. and have been extensively studied for more than fifteen years. Usually, as a magneto-active layers in these structures Bi-substituted yttrium iron garnet films (Bi: YIG) of thin and ultrathin thickness are used.

In this respect, the extraordinary interest caused (Bi,Ga)-substituted DyIG [(Bi,Ga:DyIG)] films, having a rather unique combination of positive uniaxial anisotropy, large intrinsic MO activity and low optical loss in the visible and near-infrared wavelength region of optical spectrum. All these properties can be controlled in wide range by varying both the composition of the films and the conditions of their growth. In addition to all other characteristics, it is very important to know the surface state (roughness parameters and a grain sizes) of these films.

Pulsed laser deposition (PLD) [7,8], radio frequency magnetron sputtering (RFS) [9–17] as well as reactive ion-beam sputtering (RIBS) [18] are the widely used vacuum methods for Bi Ga:DyIG films preparation as well as for Bi: YIG garnet films of another composition. PLD is mainly used for in situ epitaxial growth of the films and all-garnet 1D-MPCs, RFS and RIBS – for in situ epitaxial growth, and the two-stage one, i.e. sputtering and subsequent crystallization in oxygen or atmosphere.

As it has been shown in a number of early studies [9–12], Bi-substituted garnet films have attracted much attention for a high density magneto-optical recording materials because of their strong magneto-optical effect at short wavelengths near 500 nm.

The polycrystalline $(BiDy)_3(Fe, Al \text{ or } Ga)_5O_{12}$ garnet films of good quality with stress-induced magnetic anisotropy normal to the film plane prepared by RFS method on glass substrates using pure Ar or $Ar + O_2$ as the sputter gas were proposed for MO storage with ultra-high density MO recording [9–11]. However, it's well known that the polycrystalline films have a serious problem of suffering from the media noise due to grain boundary and microstructure inhomogeneity and the epitaxial films with high crystallographic quality can be grown by RFS only on single crystal substrates.

A rapid thermal anneal for forming $(BiDy)_3(FeGa)_5O_{12}$ films of garnet phase deposited by RFS was employed by the authors of [12]. It was found the crystallization mechanism is the diffusion controlled growth of a fixed number of crystallites, irrespective of the shape of the crystallites, provided that the shape doesn't change during growth. The grain size obtained by analyzing the X-ray diffraction linewidths was found to be consistent with such observations and decreases from 70 nm at $r = 1\,^{\circ}C/s$ to 30 nm at $r = 50\,^{\circ}C/s$, where r is a ramp-up rate.

Almost all researchers note the extreme sensitive of the composition and structure of growing films to substrate

* Corresponding author at: Vernadsky Ave., 4, Simferopol, 295007, Russia.
E-mail address: shalex53@gmail.com (A.N. Shaposhnikov).

http://dx.doi.org/10.1016/j.materresbull.2017.06.036
0025-5408/

temperature, oxygen pressure and the annealing process durations as well as substrate material. For example, according to X-ray diffraction the films of average composition $Bi_{1.5}Dy_{1.5}Fe_{4.0}$ $Ga_{1.0}O_{12}$ grown by PLD method on GGG (111) and (110) had a single garnet phase with [111] and [110] orientation, respectively, perpendicular to the film plane. The films grown on Yttria Stabilised Zirconia (100) and Si (100) substrates demonstrated the presence of randomly oriented polycrystalline garnet in addition to a small amount of other phases under constant another growth conditions [7].

Magnetically coupled double-layer $(BiDy)_3(FeGa)_5O_{12}$ garnet films of fine granular microstructure with different magnetic compensation temperatures have been prepared by PLD method varying oxygen pressure during the deposition process [8]. Authors represent a new switching system as an alternative to exchange-coupled magnetic metallic thin layers.

A series of studies [13–19] devoted to the development of technological modes of production of $(BiDy)_3(FeGa)_5O_{12}$ films, as well as composite material $(BiDy)_3(FeGa)_5O_{12}$:Bi_2O_3 with specified characteristics prepared by RFS method.

In [13,14] in order to crystallize the amorphous $Bi_2Dy_1Fe_{4-}$ Ga_1O_{12} films and nanocomposite $(BiDy)_3(FeGa)_5O_{12}$: Bi_2O_3 layers synthesized by RFS on Corning 1737 glass and on a GGG substrates into polycrystalline ferrimagnetic garnet phase, a post-deposition high temperature annealing was used with temperature ramp rates (up and down) in between 3–5 °C/min, for a number of different annealing durations. X-ray diffraction patterns reveals the nanocrystalline microstructure of the annealed garnet materials and the body-centered cubic lattice structure type, as well as only one identifiable impurity phase (Fe_3O_4) being present residing outside garnet grains.

Manufactured by RFS method $Bi_2Dy_1Fe_4Ga_1O_{12}$ films of thicknesses between 50 and 5000 nm with typically root main square roughness (RMS) about 2 nm across a randomly-selected film area of 1 μm^2 possessed a sufficient level of uniaxial magnetic anisotropy in a direction perpendicular to the film plane and the properties achieved in these garnet layers makes them very attractive for use in nanostructured photonic devices and sensors [15].

Experimental study of triple-layer all-garnet heterostructures was carried out in [16]. Authors demonstrated a new material system possessing a combination of high specific Faraday rotation, a nearly rectangular magnetic hysteresis loop and low coercivity. The deposited films were annealed in air atmosphere at temperatures from 600 to 700 °C, and the annealing process durations varied between 30 min and 12 h. Note that such a long time of annealing can be harmful to oxide dielectric mirrors in the relevant structures.

In [17] the microcrystalline structure with small grain size, high volumetric content of garnet phase and low surface roughness was achieved in the magnetic garnet layers $Bi_2Dy_1Fe_4Ga_1O_{12}$ by depositing additional non-magnetic garnet layers (GSGG), which protect the magnetic garnet layers from the atmospheric exposure using complex multi-step rapid thermal annealing processes. Sputtered polycrystalline bismuth-doped iron garnet layers having grain dimensions of the order of 50 nm.

The destructive influence of garnet annealing on optical responses of dual cavities have been found in [20,21]. To avoid formation of cracks, the authors used the $(GdCa)_3(GaMgZr)_5O_{12}$ substrates with the coefficient of thermal expansion similar to that of Bi: YIG. To crystallize Bi: YIG, the samples were annealed at 700 °C for 15 min. Annealing determined the surface roughness after crystallization: RMS = 0.2 nm (before) and RMS = 2.8 nm (after).

Another way to avoid the degradation of properties of dielectric Bragg mirrors in of 1D-MPCs due to thermal annealing of Bi: YIG films is the laser annealing of such films [22].

Therefore, the aim of this work was to choice the parameters of crystallization annealing of Bi,Ga:DyIG films, which would allow obtaining films with satisfactory optical (transmission), magneto-optical (specific Faraday rotation), structural (degree of crystallinity) and surface roughness characteristics (RMS) on GGG and CMZGGG substrates.

2. Experimental

Bi,Ga:DyIG films of 120 nm thick of composition $Bi_{2.3}Dy_{0.7-}$ $Fe_{4.2}Ga_{0.8}O_{12}$ were deposited on hot (350 °C) substrates of single-crystal gadolinium–gallium (GGG) and calcium-magnesium-zirconium-gadolinium–gallium (CMZGGG) garnets by RIBS technique in argon–oxygen mixture in relation of 70 and 30%, correspond-

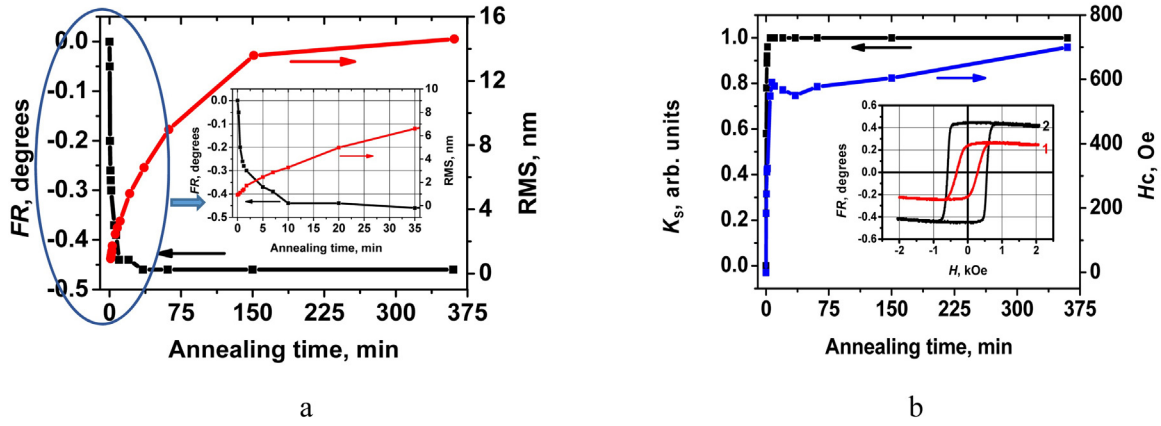

Fig. 1. Θ_F and RMS (a) and K_S and Hc (b) dependencies on annealing time. The inset: (a) – the same dependencies on an enlarged scale on the X-axis; (b) – FLHS for the films annealed at t = 1.2 (red, curve 1) and 5 (black, curve 2) min. (For interpretation of the references to colour in this figure legend, the reader is referred to the web version of this article.)

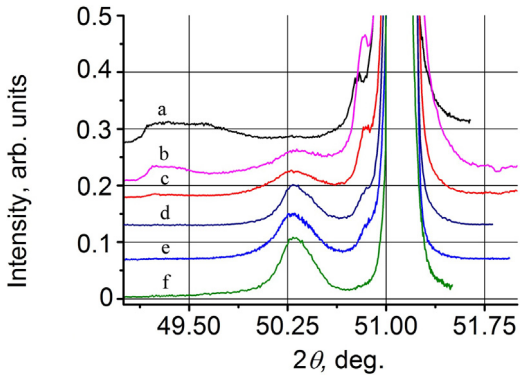

Fig. 2. The normalized XRD patterns in CuKα radiation of Bi,Ga:DyIG films, prepared on a GGG substrates and annealed different time: a – 1.2 min (black); b – 5 min (magenta); c – 20 min (red); d – 60 min (dark blue); e – 150 min (blue); f – 360 min (olive). (For interpretation of the references to colour in this figure legend, the reader is referred to the web version of this article.)

ingly, with following crystallization by high temperature annealing in the air at atmospheric pressure as described earlier [23,24]. The samples on GGG substrates are named as S_{GGG}-number and on CMZGGG substrates as S_{CMZ}-number.

The compositions of the films were chosen to obtain the films with high value of out of plane magnetic anisotropy, desired Faraday rotation angle Θ_F and rectangular hysteresis loop (i.e. values of squareness ratio as relation of residual values of Θ_F to saturation one must be $K_S = 1$). The targets for sputtering were prepared using conventional ceramic technique. The as-sputtered Bi,Ga:DyIG films were amorphous and to crystallize ones a post-deposition annealing at 700 °C was carry out. The crystallization

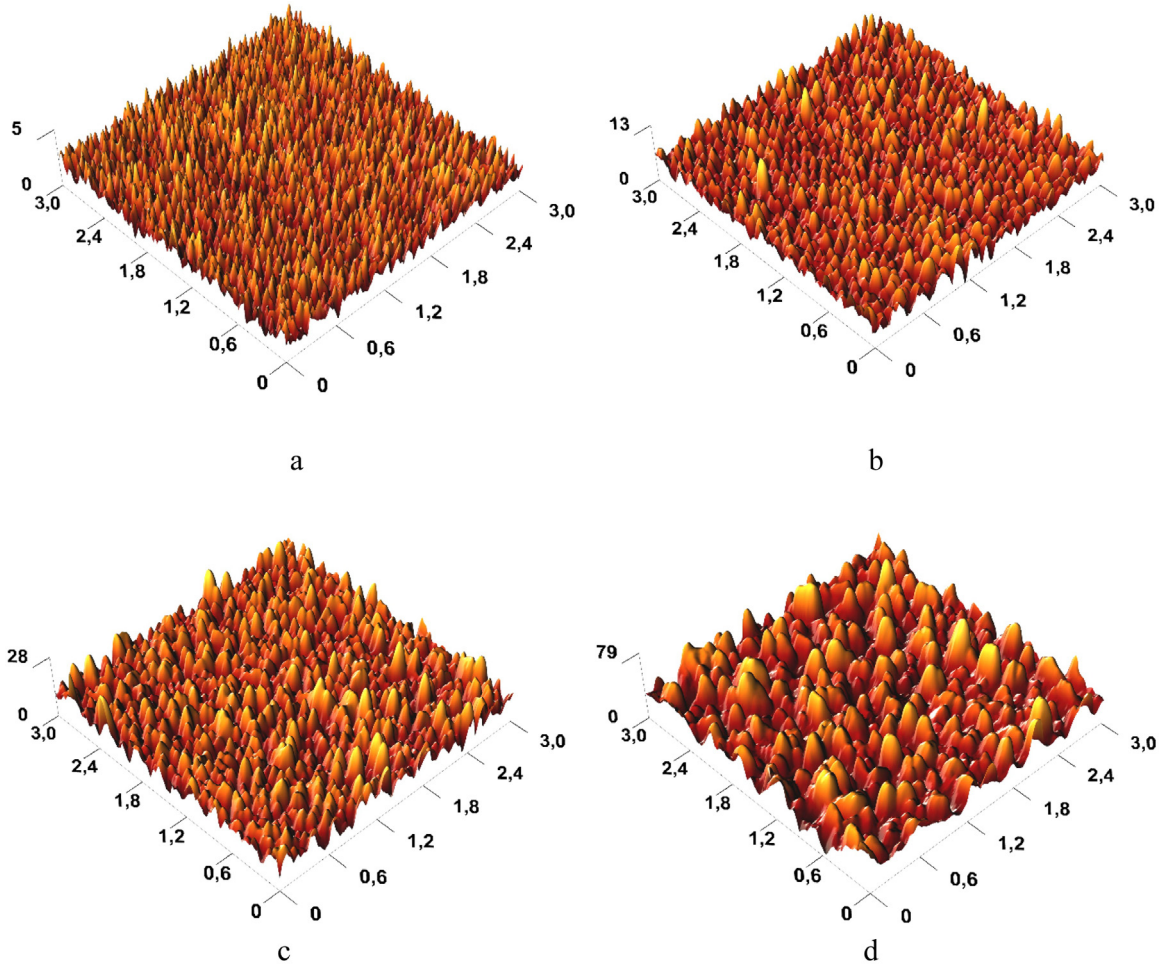

Fig. 3. AFM- surface images of Bi,Ga:DyIG films on GGG substrates after different time of crystallization annealing: a- 1.2; b – 5; c – 20; c – 60 min.

Table 1
The X-ray diffraction data for Bi,Ga:DyIG films prepared on a GGG substrates.

Sample	Annealing time, min	a_{film}, nm	Δa, nm	$\Delta a/a_{sub}$, %	FWHM, deg	RMS, nm
S_{GGG}-01	1.2	–	–	–	–	1.40
S_{GGG}-02	5.0	1.2555	0.0168	1.36	1.37	1.73
S_{GGG}-03	20.0	1.2555	0.0169	1.36	1.35	2.46
S_{GGG}-04	60.0	1.2556	0.0169	1.36	1.30	4.98
S_{GGG}-05	150.0	1.2556	0.0168	1.36	1.06	14.09
S_{GGG}-06	360.0	1.2556	0.0168	1.36	0.89	14.62

a_{film} is a film lattice parameter; Δa is a mismatch of the film and substrate lattice parameters; FWHM is a full width at half maximum; RMS is a root main square.

annealing was performed in a hand-made vertical type silit electrical furnace. The durations of the crystallization annealing process varied from 30 s to 6 h for the films on GGG substrates and to 12 h for the films on CMZGGG substrates.

To determine the magneto-optical properties of the films (Faraday rotation angle Θ_F, coercivity force Hc, squareness ratio K_S and others) the Faraday hysteresis loops (FHL) were measured using hand-made computer control magneto-polarimeter at a fixed radiation wavelength of 655 nm. The magneto-polarimeter is based on an azimuthal modulation technique and contains the following optical element sequence: 50 mW 655 nm laser – polarizer (Glan-Thompson prism) – ac Faraday-rotation modulator with Bi-substituted LPE garnet film as a magneto-active element – electromagnet with a sample – dc Faraday-rotation compensator – analyzer (Glan-Thompson prism) – photo detector.

The surface topography and the domain structure of the films were determined in a tapping mode using atomic force microscope (AFM) Ntegra Prima manufactured by NT-MDT company (Russia). A tapping mode is most preferable to investigations because it allows one to get the best value of resolution and minimize the negative impacts of the probe and the sample one each other. In this mode, the cantilever console varies with self-resonant frequency and high amplitude (approximately 50–100 nm). At these amplitudes, the needle contacts the sample surface at the moment of maximum deflection of the console down from its equilibrium position, which significantly changes the frequency, phase and amplitude of its oscillations. A tapping mode has a higher horizontal resolution compared to the contact mode.

The diffraction patterns were measured using multifunctional X-ray analytical system CompleFlex manufactured by CDP Company (Russia) [25].

In this system X-ray optical scheme of Bragg-Brentano is realized. X-ray copper tube with operating power of 280 W and a working focus projection 20 μm is used. So, the required level of angular resolution and signal intensity may be achieve without using a complex system of collimation and focusing of x-ray radiation. X-ray wavelength λ (CuK_α) is 0.1541 nm. Ni-filter is used for the cut-off a CuK_β characteristic line signal. The diffraction patterns obtained in the mode of θ–2θ scan for symmetric Bragg reflection (444). For the film structure and the substrate the rocking curves of diffraction reflections were measured too in the ω- scan mode at a fixed detector position.

3. Results and discussion

Fig. 1(a) presents the dependencies of Faraday rotation angle Θ_F and RMS on a time of crystallization annealing for Bi,Ga:DyIG films on GGG substrates. The inset shows the same dependencies on an enlarged scale on the X-axis. As one can see Θ_F almost reaches saturation after 10 min of annealing, wherein RMS is 3.3 nm. After 360 min of annealing Θ_F increased slightly, while RMS reached up to 14.62 nm.

Fig. 1(b) shows the dependencies of coercivity force Hc and squareness ratio K_S on annealing time of these films. At low annealing time, the dependence of K_S on the annealing time is a very sharp: $K_S = 1$ already after 5 min (see inset in on Fig. 1b, where the FLHS for the films annealed at $t = 1.2$ (red) and 5 (black) min are displayed), while Hc reaches a maximum value of 700 Oe after 360 min of annealing.

In Fig. 2a–e the diffraction patterns of the samples crystallized within, respectively, 1.2, 5, 20, 60, 150 and 360 min are present. In the diffraction pattern of the sample S_{GGG}-01 (Fig. 2a) in a region of

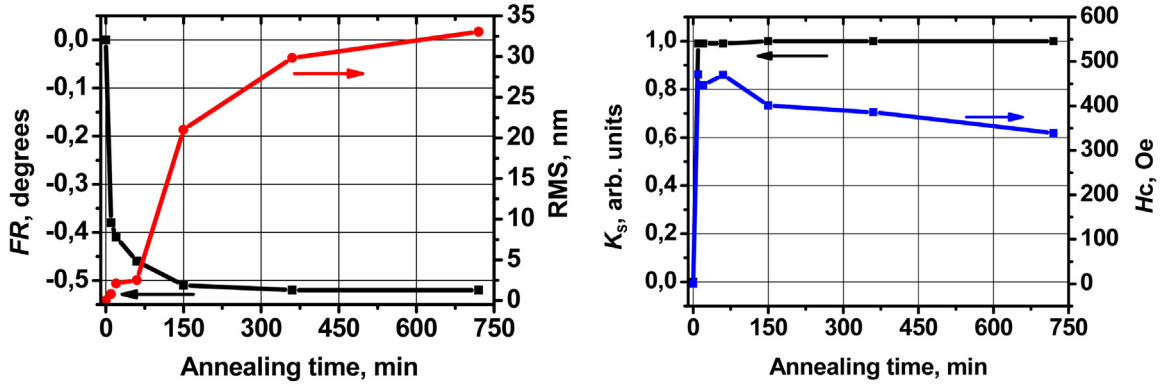

Fig. 4. Dependencies of Θ_F and RMS (a) and K_S and Hc (b) on a crystallization annealing time for Bi,Ga:DyIG films on CMZGGG substrates.

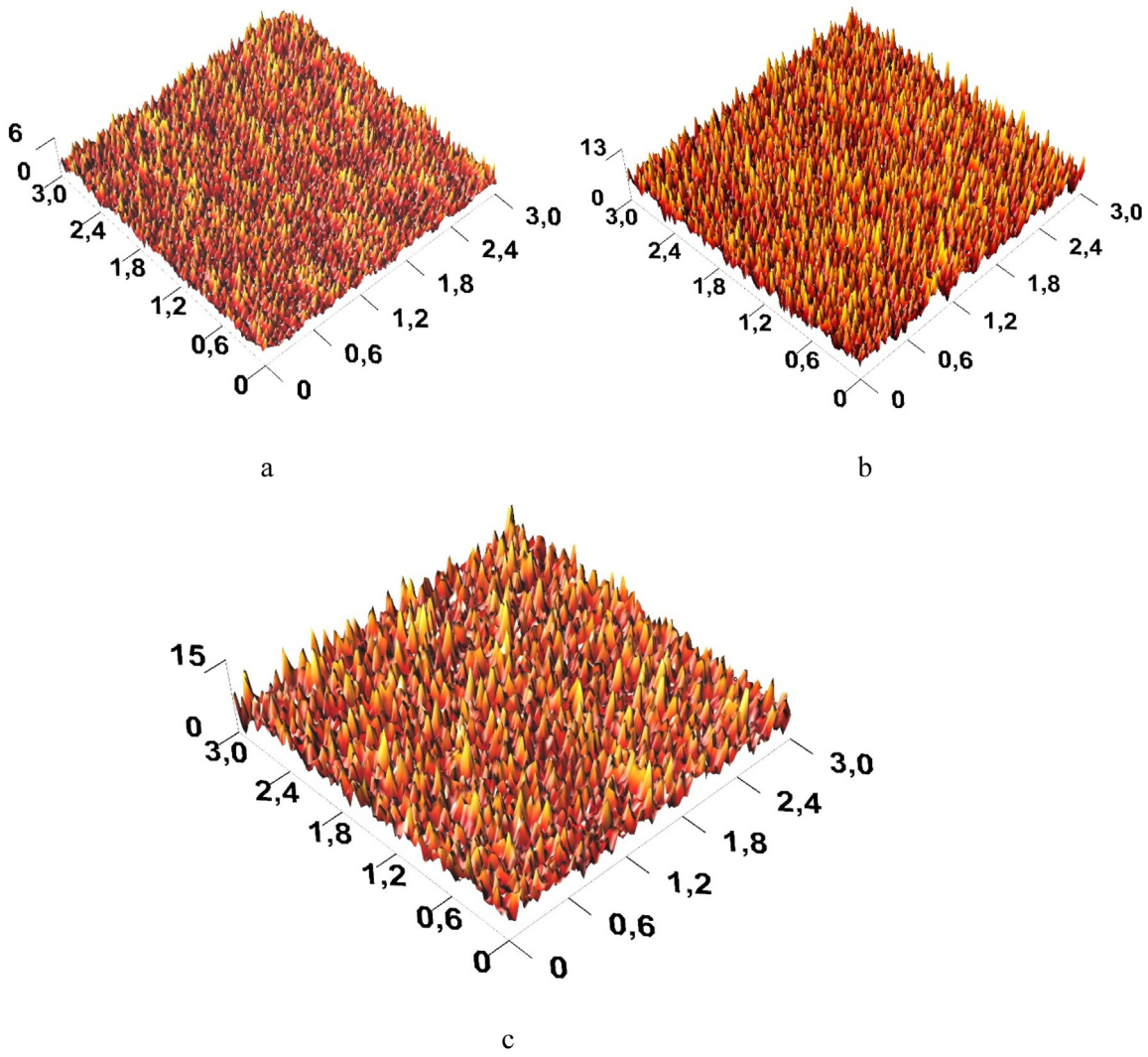

Fig. 5. AFM- surface images of Bi,Ga:DyIG films on CMZGGG substrates after different time of crystallization annealing: a – 10 min; b – 20 min; c – 60 min.

the Bragg diffraction angles $2\theta = 48.0 - 49.8^{\circ}$ a pronounced diffuse plateau is observed; at $2\theta_B = 50.3$ deg the weakly expressed diffraction peak from Bi,Ga:DyIG film is clearly seen, indicating the beginning of initial stage of the film crystallization process. The peak on the left wing of the substrate diffraction peak is due to the fine structure of a CuK_α characteristic line and owned by its satellite (measurements were carried out in a scheme without the radiation monochromatization). The diffractograms (Fig. 2) present normalized peak intensities from the film structure, so with an increase of the deposited layer crystallinity and its diffraction intensity, the CuK_α satellite peak becomes indistinguishable.

Unlike the sample S_{GGG}-01, in the diffraction pattern of the sample S_{GGG}-02 (Fig. 3b) there is a pronounced peak of Bi,Ga:DyIG films. The full width at half maximum (FWHM) of the rocking curve is quite large (FWHM = 1.37°). The FWHM of the rocking curve is determined by the magnitude of the diffuse scattering of X-rays and depends on the structural density of dislocations, the presence of micro-inhomogeneity etc. Therefore, its high value for S_{GGG}-02 indicates a high density of structural defects in the formed polycrystalline layer and incompleteness of crystallization process. For sample S_{GGG}-03 (Fig. 3c) the same pattern is seen as for S_{GGG}-02, however, the right and left "shoulders" of the diffraction peak are less pronounced, indicating a greater stress relaxation in the structure.

The diffraction pattern changes completely for the samples crystallized at annealing times $t = 60$ min or more. At $t = 360$ min the diffraction peak of the sample S_{GGG}-06 is fully resolved (Fig. 2f), the right and left "shoulders" are absent, FWHM = 0.89 deg. Thus, through prolonged annealing time the residual stresses relaxed and the structural defect density decreased. *Hc* and RMS for these films accepted the maximal values of 700 Oe and 14.6 nm, respectively, of the entire series of the samples on GGG substrates.

The X-ray diffraction data for Bi,Ga:DyIG films prepared on a GGG substrates are present in Table 1.

The measured FLHS (the inset in Fig. 1b) and X-ray diffraction data (Fig. 2) correlate well with AFM- ones. Fig. 3 shows AFM-surface images of Bi,Ga:DyIG films on GGG substrates after different time of crystallization annealing. Pictures illustrate the dynamics of growth of the film roughness with increasing of annealing time. Fine grain structure of the films with increasing of t is gradually becoming a large-block, average crystallite size at their base increases from 100 at $t = 1.2$ min to 200–250 nm at $t = 360$ min.

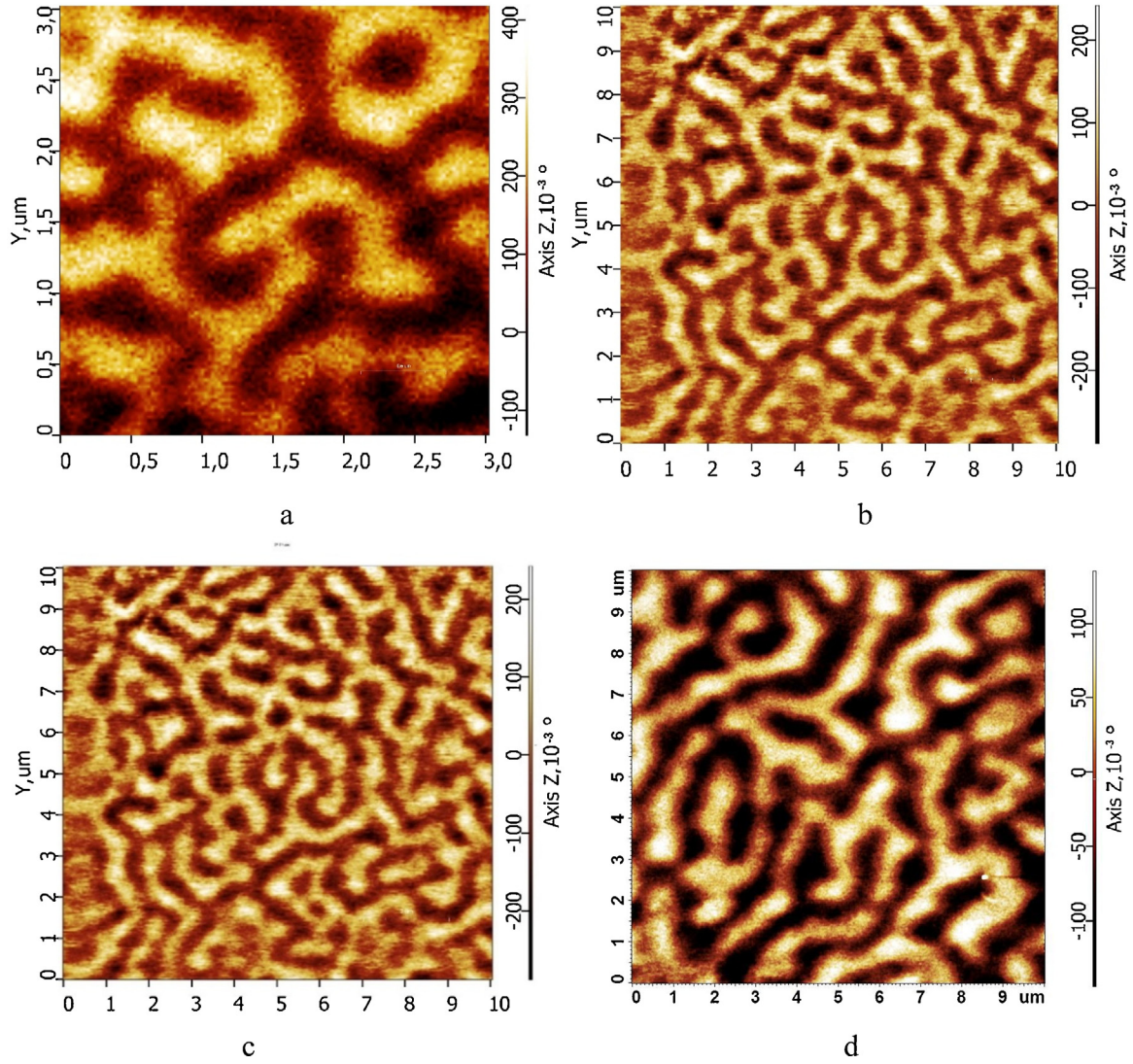

Fig. 6. MFM images of domain structures of Bi,Ga:DyIG films on GGG (a-c) and CMZGGG (d) substrates annealed different times: a – 1.2; b – 5; c – d – 20 min.

To determine the effect of the substrate material (the mismatch of crystal lattices of the substrate and the film) on the surface roughness and other film characteristics the number of films were deposited and crystallized on CMZGGG substrate. Due to the proximity of the diffraction peaks of the film and CMZGGG substrate to measure correctly rocking curves and obtain the value of FWHM was impossible.

Fig. 4(a) presents dependencies of Faraday rotation angle Θ_F and RMS on a crystallization annealing time of Bi,Ga:DyIG films on CMZGGG substrates. As one can see, Θ_F do not reaches saturation yet after 60 min of annealing, wherein RMS is 2.51 nm. Θ_F reaches saturation only at $t \geq 360$ min. These films acquired the block structure, average crystallite size at their base reached 250–300 nm, RMS was 32.6 nm, however unlike the films on GGG substrates, in the time region $0 < t < 60$ min Hc first increases and then decreases with t increasing at $t = 720$ min Hc reached 340 Oe (Fig. 4b).

Bragg diffraction angle for the Bi,Ga:DyIG films on CMZGGG substrates is $2\theta_B = 50.26^\circ$, so, calculated lattice parameter is $a_{Film} = 1.2567$ nm and this means that $\Delta a = 0.0073$ that is 2.3 times less than on GGG substrate. Due to the proximity of the diffraction peaks of the film and CMZGGG substrate it was not possible to measure the rocking curves for the films and determine their FWHM.

Calculation of the target lattice parameter a_{Target} in accordance with the nominal composition of the target and Vegard's law [26] have shown that $a_{Target} = 1.2567$ nm. This indicate about identical compositions of the target and the films on CMZGGG substrates, i.e. during sputtering process almost 100% – th mass transfer of the target material occurs to the substrate, and during crystallization annealing the garnet phase of the same composition is formed on CMZGGG substrate.

Fig. 5 shows AFM- surface images of Bi,Ga:DyIG films on CMZGGG substrates after different time of crystallization annealing. As can be seen, the films have fine texture even after annealing during 60 min.

In contrast to the results obtained in [12], not only the size of crystallites, but also their density significantly depend on the annealing time. The increasing of annealing time leads to an increase in crystallite size due to their merger, the crystallites form remains the same. The similar results were obtained in [27] during

crystallization annealing of the RIB sputtered films of composition $Bi_{2.8}Y_{0.2}Fe_5O_{12}$.

The magnetic domain structures of Bi,Ga:DyIG thin films on GGG and CMZGGG substrates annealed different times in the absence of externally applied magnetic fields are shown in Fig. 6. The domain patterns were observed using a MFM-mode of SPM microscope.

Bi,Ga:DyIG films are high-coercivity ones and after magnetization usually tend to remain in a single-domain state. For observation of the domain structure (DS) of such films, the demagnetization process by heating above the Neel temperature and cooling in the absence of external magnetic field was carried out. DS of Bi,Ga:DyIG films is similar to the classic one of LPE garnet films that clearly indicates the crystallinity of the ferrite-garnet phase of the films. However, for the films on GGG substrates with low annealing time (Fig. 6a–b) a fine magnetic structure (substructure) is observed on the background of a uniformly magnetized domains. The emergence of such domain substructure (dots, ripples, domain size of less than 100 nm) can be attributed to the formation of reverse magnetic phase germs with the magnetic moment concentrated on such irregularities in zero magnetic field ($Ks < 1$ – see inset in Fig. 1, as well.). Increasing of annealing time results in decreasing of the average domain width W ($W = 0.5\ \mu m$ at $t = 1.2$ min and $W = 0.3\ \mu m$ at $t = 20$ min) and improving the uniformity of their magnetization, which indicates the increasing the degree of the film single-crystallinity (see Fig. 6c).

For the films on CMZGGG substrates $W = 0.7\ \mu m$ at $t = 20$ min that may indicate a different value of uniaxial magnetic anisotropy of the films on GGG and CMZGGG substrates. Indeed, the measurements of the uniaxial anisotropy field H_A showed that under the same annealing time the uniaxial anisotropy field H_A of the films on GGG is higher than the films on CMZGGG substrates. As well if annealing time increases H_A of the films on GGG increases and on CMZGGG substrates decreases. This fact explains the course of the time dependency of Hc of the films on booth types of substrates (See Figs. Fig. 11b and Fig. 44b).

It may be note that the enlargement of projecting crystallites leads to “microdomains” which enhance the contrast, but not change the magnetization.

Bi,Ga:DyIG films on GGG substrates are in a stressed (compressed) state due to large lattice mismatch $\Delta a = 0.0168$ nm. This leads to a blurring of the domain walls (Fig. 6a–c). In Bi,Ga:DyIG films on CMZGGG substrates $\Delta a = 0.0073$ nm, so, a stressed state is much less. This affects the texture of the films and character of the domain walls – they are more consistent with the domain walls of LPE garnet films (Fig. 6d).

4. Summary

The roughness of Bi,Ga:DyIG films on GGG and CMZGGG substrates increases with increasing of annealing time, their surface texture changes from fine to large-block. At annealing time up to 60 min the roughness of the films on CMZGGG substrates is substantially lower than on GGG one. The mismatch of lattice parameters of the films on GGG and CMZGGG substrates after annealing at $t \geq 5$ min independent of annealing time and on GGG substrates is +0.0168 nm, and on CMZGGG substrates is 0.0073 nm. Thus, the stress component in the films on GGG substrates is higher, which explains the increased roughness of the films on GGG substrates compared with films on CMZGGG ones at the same t.

Under the same annealing time the uniaxial anisotropy field H_A of the films on GGG substrates is higher than the films on CMZGGG ones. If annealing time increases H_A of the films on GGG increases and on CMZGGG substrates decreases.

There is an optimal time of annealing for the films on both types of substrates (from 10 to 20 min) at which a compromise between the magneto-optical characteristics from one side and surface roughness parameters from other one is reached.

Acknowledgments

This work is support by the RF Ministry of Education and Science (project no. 3.7126.2017).

In a part of structural XRD measurements and its discussions and conclusions, made by

N. Gerasimenko and D. Smirnov, the work was supported by the Russian Scientific Foundation (project no. 15-19-10054).

References

[1] Jae-Hyuk Park, H. Takagi, K. Nishimura, H. Uchida, M. Inoue, Jae-Hak Park, Jae-Kyeong Cho, Magneto-optic spatial light modulators driven by an electric field, J. Appl. Phys. 93 (2003) 8525–8527.
[2] K.H. Chung, J. Heo, K. Takahashi, S. Mito, H. Takagi, J. Kim, P.B. Lim, M. Inoue, Characteristics of magneto-photonic crystals based magneto-optic films for spatial light phase modulators, J. Magn. Soc. Jpn. 32 (2008) 114–116.
[3] H. Kato, M. Inoue, Reflection-mode operation of one-dimensional magnetophotonic crystals for use in film-based magneto-optical isolator devices, J. Appl. Phys. 91 (2002) 7017–7019.
[4] H. Kato, T. Matsushita, A. Takayama, M. Egawa, K. Nishimura, M. Inoue, Properties of one-dimensional magnetophotonic crystals for use in optical isolator devices, IEEE Trans. Magn. 38 (2002) 3246–3248.
[5] M. Inoue, M. Levy, A.V. Baryshev, Magnetophotonics: From Theory to Applications Springer Series in Materials Science, (2010) .
[6] M. Vasiliev, V.A. Kotov, K. Alameh, V.I. Belotelov, A.K. Zvezdin, Novel magnetic photonic crystal structures for magnetic field sensors and visualizers, IEEE Trans. Magn. 44 (2008) 323–328.
[7] P. Papakonstantinou, B. Teggart, R. Atkinson, Characterization of pulsed laser deposited Bi doped Dy iron garnet thin films on GGG(111), GGG(110), YSZ(100) and Si(100), J. Phys. IV France 7 (1997) (C1-475-476).
[8] M. Kučera, R. Gerber, B.J. Teggart, Magnetization reversal in coupled magneto-optical BiDy-iron garnet films, JMMM 219 (2000) 241–247.
[9] M. Gomi, M. Abe, Sputtered iron garnet films for magneto-optical storage, Mat. Res. Soc. Symp. Proc. 150 (1989) 121–130.
[10] M. Gomi, K. Utsugi, M. Abe, RF sputtered films of Bi-substituted garnet for magneto-optical memory, IEEE Trans. Magn. 22 (1986) 1233–1235 (MAG).
[11] M. Gomi, T. Tanida, M. Abe, RF sputtering of highly Bi-substituted garnet films on glass substrates for magneto-optical memory, J. Appl. Phys. 57 (1985) 3888–3890.
[12] T. Suzuki, G. Zaharchuk, G. Gonnan, F. Sequeda, P. Labun, Magnetic and magneto-optical properties and crystallization kinetics of rapid-thermally crystallized Bi-substituted garnet films, IEEE Trans. Magn. 26 (1990) 1927–1929.
[13] M. Nur-E-Alam, M. Vasiliev, K. Alameh, V.A. Kotov, Physical properties and behaviour of highly Bi-substituted magneto-optic garnets for applications in integrated optics and photonics, Adv. Opt. Technol. 2011 (2011) 971267.
[14] M. Vasiliev, M. Nur-E-Alam, V.A. Kotov, K. Alameh, V.I. Belotelov, V.I. Burkov, A. K. Zvezdin, RF magnetron sputtered $(BiDy)_3(FeGa)_5O_{12}$:Bi_2O_3 composite garnet-oxide materials possessing record magneto-optic quality in the visible spectral region, Opt. Express 17 (2009) 19519.
[15] M. Vasiliev, K. Alameh, V. Kotov, Doped Iron Garnet Materials for Magnetic Photonic Crystals, Edith Cowan University Research Online ECU Publications, 2008. http://ro.ecu.edu.au/ecuworks/803.
[16] V.A. Kotov, A.F. Popkov, S.V. Soloviev, M. Vasiliev, K. Alameh, M. Nur-E-Alam, D. E. Balabanov, Magnetic heterostructures with low coercivity for high-performance magneto-optic devices, J. Phys. D: Appl. Phys. 46 (2013) 035001 (9pp).
[17] M. Vasiliev, P.C. Wo, K. Alameh, P. Munroe, Z. Xie, V.A. Kotov, V.I. Burkov, Microstructural characterization of sputtered garnet materials and all-garnet magnetic heterostructures: establishing the technology for magnetic photonic crystal fabrication, J. Phys. D: Appl. Phys. 42 (2009) 135003 (9pp).
[18] M. Nur-E-Alam, M. Vasiliev, V.A. Kotov, K. Alameh, Garnet Multilayer Thin Film Structure with Magnetostatically-Altered and Improved Magnetic Properties Prepared by RF Magnetron Sputtering, IEEE. Published in: High Capacity Optical Networks and Enabling Technologies (HONET), 2011, pp. 6149812.
[19] M. Nur-E-Alam, M. Vasiliev, K. Alameh, Synthesis, characteristics, and material properties dataset of Bi:DyIG-oxide garnet-type nanocomposites, J. Nanomater. (2015) 127498, doi:http://dx.doi.org/10.1155/2015/127498.
[20] T. Goto, A.V. Baryshev, K. Tobinaga, M. Inoue, Faraday rotation of a magnetophotonic crystal with the dual-cavity structure, J. Appl. Phys. 107 (2010) 09A946.

[21] Y. Haga, T. Goto, A.V. Baryshev, M. Inoue, One-dimensional single- and dual-cavity magnetophotonic crystals fabricated by bounding, J. Magn. Soc. Jpn. 36 (2012) 54–57.
[22] Y. Susuki, Y. Eto, K. Yamada, T. Goto, H. Takagi, P.B. Lim, A.V. Baryshev, M. Inoue, Fabrication of garnet-based magnetophotonic crystals by means of laser annealing technique, Magnetics and Optics Research Intern. Symp. (MORIS 2011), Nijmegen, Netherlands, 21–24 June 2011: book of abstr. – [S. l.], 2011, pp. 116.
[23] V.N. Berzhansky, A.N. Shaposhnikov, A.R. Prokopov, A.V. Karavainikov, T.V. Mikhailova, E.Y. Semuk, M.I. Sharipova, T.V. Dolgova, A.A. Fedyanin, V.A. Kotov, V.O. Golub, One-dimensional magnetophotonic crystals based on double-layer Bi-substituted iron garnet films, Mat.-wiss. u. Werkstofftech. 42 (2011) 19–23.
[24] V.N. Berzhansky, T.V. Mikhailova, A.V. Karavainikov, A.R. Prokopov, A.N. Shaposhnikov, I.N. Lukienko, Yu N. Kharchenko, O.V. Miloslavskaya, N.F. Kharchenko, Microcavity one-dimensional magnetophotonic crystals with double layer iron garnet, J. Magn. Soc. Jpn. 36 (2012) 42–45.
[25] N.N. Gerasimenko, D.I. Smirnov, A.G. Touryanski, New X-ray measuring system with microfocus sources for the diagnosis of solid micro- and nanostructures, Nanoindustry 56 (2015) 58–69.
[26] A.R. Denton, N. WE. Ashcroft, Vegard's law, Phys. Rev. A 43 (1991) 3161.
[27] A.N. Shaposhnikov, A.R. Prokopov, A.V. Karavainikov, V.N. Berzhansky, T.V. Mikhailova, V.A. Kotov, D.E. Balabanov, I.V. Sharay, O.Y. Salyuk, M. Vasiliev, V.O. Golub, Modification of Bi:YIG film properties by substrate surface ion pre-treatment, Mat. Res. Bull. 55 (2014) 19–25.